An efficient method for water content estimation of building materials from spectral reflectance

Bikram Koirala, Paul Scheunders

[a] *University of Antwerp, Universiteitsplein 1, Antwerp, Belgium*

Abstract

We propose a nondestructive methodology to accurately estimate the water content of building materials from spectral reflectance in the shortwave infrared. The water content of a wet sample is estimated from the relative position of its reflectance spectrum on the curve between 2 reference spectra with known water content. By design, the approach is invariant to variations in illumination and acquisition conditions. Validation is done on datasets of clay powders and bricks. The experimental results provide confirmation of the effectiveness of the proposed method.

Keywords: Remote sensing, Hyperspectral, Water content, Clay, Brick, Cultural heritage

1. Introduction

The determination of water content is often a critical component in production processes and quality assurance. The most accurate approach to estimate the water content (WC) of wet samples is the gravimetric method, in which a small amount of wet material sample is weighted and oven-dried until no further loss of mass is observed. The WC of the sample is then obtained from the weight difference between the wet and oven-dried sample. This technique is reliable and very accurate (error of <0.1 g/g $\times$ 100 WC). The major disadvantage of this approach is that it is destructive (heating) and very time-consuming (hours to dry the sample), making it impractical for industrial applications requiring continuous monitoring. For these types of applications, non-destructive methodologies must be developed.

Different nondestructive methods have been developed for WC estimation of building materials [1], with various sensor principles, including microwave

reflectometry [2], terahertz imaging [3], neutron radiography [4] and NMR spectrometry [5].

It is widely recognized that the WC of materials significantly impacts the reflectance of material surfaces within the visible near-infrared (VNIR) (400–1000 nm) and the short-wave infrared (SWIR) (1001–2500 nm) wavelength regions [6, 7]. In particular, the optical properties of water-bearing materials are dominated by water in the SWIR. In the remote sensing domain, hyperspectral imaging has been applied for several decades to estimate water content in leaf and canopy [8, 9] and soil [10, 11]. Despite the limited penetration depth of light (ranging from a few micrometers to a few millimeters) in this wavelength region, hyperspectral imaging allows the determination of WC of the upper layer of soil at a high spatial resolution [12]. The major advantage of using this spectral range in remote sensing applications lies in the fact that solar radiation serves as a natural source of illumination.

Since the WC is one of the parameters that influence the quality of building materials, the potential of hyperspectral imaging as a non-destructive measurement method has been recognized. In [13], hyperspectral imaging was shown to be more reliable than the standard water indicator to evaluate the penetration depth of rain water in cement mortar incorporating blast furnace slag. In [14], liquid phase moisture transport through cement mortar was studied using near-infrared spectroscopy. In [15], concrete samples were classified based on their initial water-to-cement ratios using a SWIR spectrometer. It is a generally accepted fact that the degree of compaction of subgrade soil is significantly influenced by its WC. In [16], the estimation of ground WC was achieved by establishing both linear and non-linear relationships between the spectral reflectances of wet soil samples and their corresponding WC.

Although hyperspectral imaging techniques are widely used for the conservation of historic buildings, their application for analyzing the impact of water on these structures is rare. As mentioned in [17, 18], the deterioration and degradation of the materials surface in historical structures is often associated with the presence of water. The WC of porous materials plays a crucial role in the transport of gases, liquids, and ions. A recent study ([17]) analyzed reflected light from wet samples, particularly at 970 nm, to estimate the WC of porous materials.

In general, the state of the art for estimating the WC of building materials from spectral reflectance is based on qualitative or empirical methodologies. For an accurate estimation, two major challenges need to be addressed:

- Reflectance spectra suffer from spectral variability. Variations in illumination and viewing angle cause scaling of the reflectance spectra, which can occur both globally and at the pixel level. Variations in acquisition conditions, including differences in sensors and white calibration, contribute to wavelength-dependent variations in the measured spectra.

- The spectral response to water differs between materials. The spectral reflectance of wet porous materials is strongly influenced by the size and distribution of pores. These factors dictate how water is distributed within a sample. For two porous samples with identical WC, in the sample characterized by the largest pore size, the incident light travels greater distances through the water before being reflected by the sample.

In this work, we will focus on addressing these two challenges to allow an accurate estimation of the WC of wet building materials. The major assumption of the proposed method is that the data manifold sampled by a number of wet samples with varying WC is a curve between the spectra of the air-dry and saturated versions of the sample. The relative position of the reflectance spectrum of a test sample on this curve is then a measure for its WC. In [19], a similar approach was applied for unmixing of binary intimate mixtures. In that work, the relative position of a mixture was calculated using the geodesic distance between the mixture and the spectra of the two pure materials (endmembers), i.e., the extremes of the curve, and was found to be invariant to variations in acquisition conditions. In this work, we will address random scaling effects in the measured spectra while ensuring an accurate calculation of the geodesic distance, through a strategy that involves projecting all measured spectra onto the unit hypersphere. The second challenge will be addresssed by using endmembers obtained from the same material as the test sample, i.e., with a similar pore size distribution. The relative position of a test sample is then related to its actual WC by using the ground truth WC of the endmembers obtained by gravimetry. Moreover, to increase the accuracy, the endmembers do not need to be air-dry and saturated but can be any minimally wet and maximally wet sample. The proposed method will be validated on a number of self-crafted hyperspectral datasets of clay samples and bricks.

The remainder of this article is structured as follows. In Section 2, we describe the datasets on which the proposed method is validated. Section 3 is dedicated to the elaboration of the proposed methodology. In Section 4,

we outline the experiments and present the results, followed by a discussion in 5. The conclusion of this work is summarized in Section 6.

2. Data description

2.1. Wet clay samples

This dataset contains three clay powders, typically applied in building materials: Roof clay, Red clay, and Mixed clay (see Figure 1 for the RGB image). These clays predominantly consist of Aluminium silicate hydroxide, Biotite, Goethite, and Silicon dioxide (see Table 1 for the detailed information).

Figure 1: The RGB image of clay powders. Left: Roof clay; Middle: Red clay; Right: Mixed clay.

Table 1: The molecular composition of the pure clay samples studied in this research.

Molecule	**Molecular formula**	**Roof clay**	**Red clay**	**Mixed clay**
Biotite	$Si_{1.36}$ $Al_{1.24}$ $Fe_{1.4}$ $Mg_{0.71}$ $Ti_{0.16}$ $Na_{0.02}$ $K_{0.98}$ O_{12} $H_{1.64}$	10.55%	3.76%	4.38%
Goethite	FeO(OH)	1.91%	0.5%	0.27%
Kaolinite	$Al_2Si_2O_5(OH)_4$	45.32%	5.62%	39%
Silicon dioxide	SiO_2	42.23%	90.13%	56.35%

Every dry clay sample was placed into a cylindrical sample holder with an interior diameter of 20 mm, a height of 5 mm, and an edge thickness of approximately 3 mm. The sample holder was filled to 1-2 mm from the edge, compacted, and smoothed using a stamp compactor. Next, water was gently

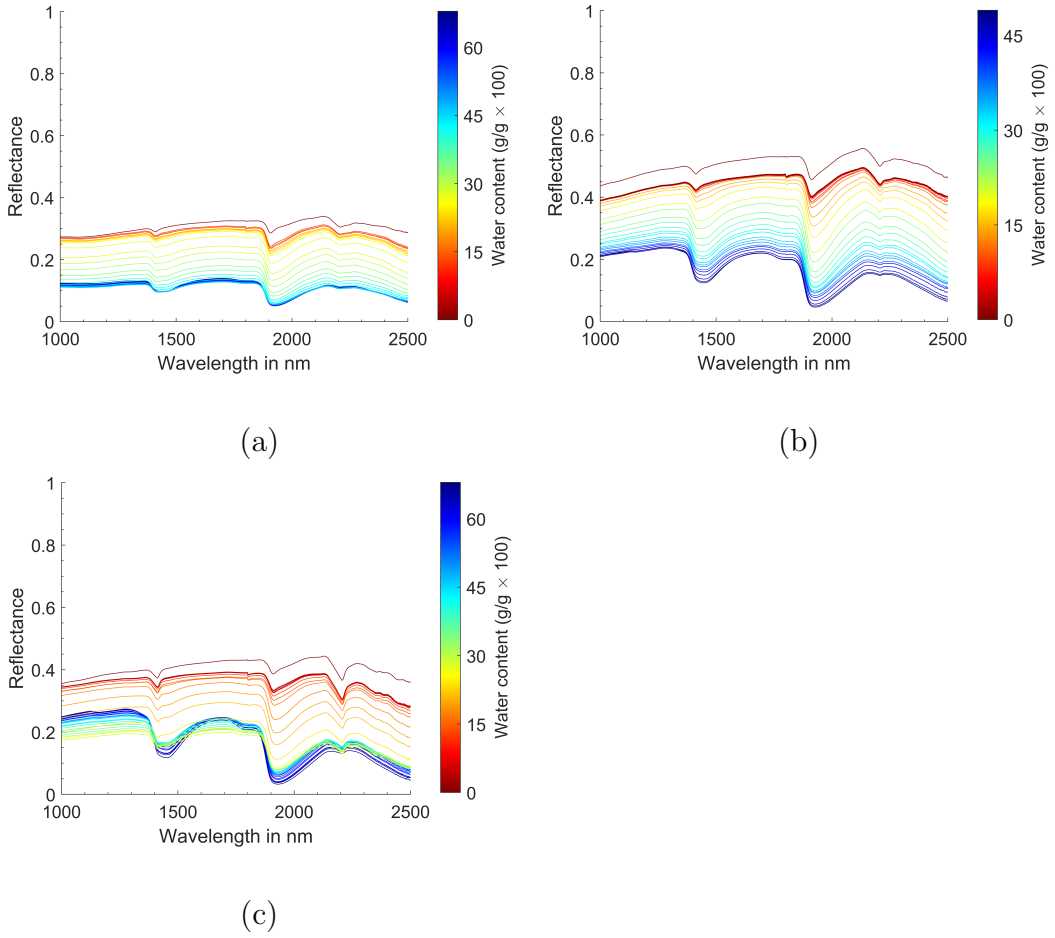

Figure 2: Measured reflectance spectra (ASD spectroradiometer) and corresponding WCs (see colorbar): (a) Roof clay, (b) Red clay, and (c) Mixed clay. The colors are scaled between 0 (dry sample) and maximum water content (saturated sample).

poured from the top until saturation (when a layer of water remains on top of the clay). Water and clay were uniformly mixed with a spatula, ensuring a homogeneous mixture. Throughout the drying process, the reflectance spectra and weight of the samples were measured consistently until the sample weight returned to its initial value (after approximately 8 h). The SWIR spectral reflectance of these samples was acquired by an AgriSpec spectroradiometer, manufactured by ASD (Analytical Spectral Devices). The spectral range of this sensor is 1001-2500 nm with a spectral sampling of 1 nm. The

time gap between two successive measurements was roughly 10 mins. The WC of a sample was obtained as:

$$\mathrm{WC} = \frac{(m - m_0)}{m_0} \times 100 \tag{1}$$

where m is the measured mass of the wet clay sample and m_0 is the initial (air-dried) mass. The Sartorius balance used in the experiment has a resolution of 0.1 mg. The spectral reflectance of all measured samples and their corresponding WC is depicted in Figure 2.

2.2. Wet built heritage sample

This dataset contains one red brick sample (approximately 3.5 × 5.5 × 6.5 cm^3) obtained from a Belgian cultural heritage site (see Figure 3 (a) for the RGB image). The brick sample is an archaeological remnants from Kipdorp, the largest archaeological site within Antwerp city. This sample

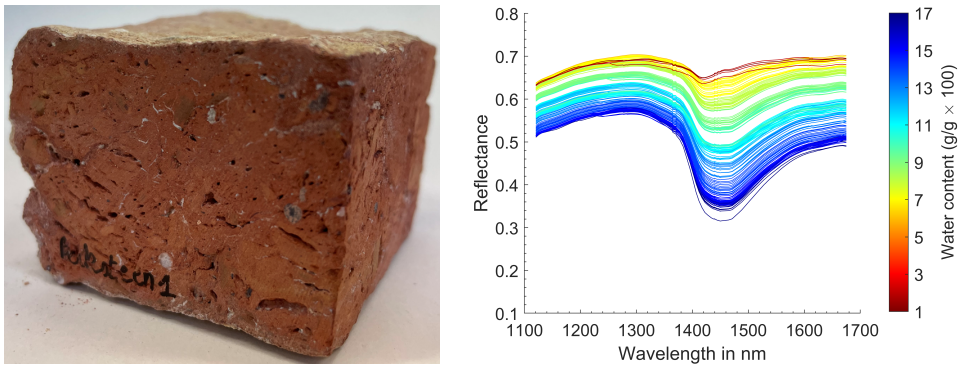

(a) (b)

Figure 3: (a) The RGB image of the built heritage sample; (b) Measured reflectance spectra (SWIR camera) and corresponding WCs (see colorbar).

was immersed in water for 2 d to ensure it is fully saturated. The spectra and weight of this sample were consistently measured until the sample weight returned to the initial value (after approximately 31 h). The samples were scanned with a snapscan hyperspectral SWIR camera (manufactured by Imec), with a spectral range spanning from 1120 to 1675 nm, a spectral resolution varying between 4-17 nm, and a total of 100 spectral bands. Since

only one side of this sample was smooth, we only scanned images from that particular side. In Figure 3 (b), the mean spectral reflectances are plotted, along with their corresponding WC.

2.3. Wet brick samples

The final dataset contains four different brick cubes (approximately 2 × 2 × 2 cm^3): Red, Yellow, Grey 1, and Grey 2 (see Figure 4 for the RGB image). In Belgium, these bricks are commonly used for the construction of walls.

Figure 4: RGB image of brick samples.

These samples were immersed in water for 2 d to ensure they were fully

saturated. The spectra and weight of the samples were measured consistently until the sample weight returned to the initial value (after approximately 7 h for each brick type). Note that the samples are not completely dry at this point, with a WC still around 2-3 (g/g $\times$100), but it would take much longer to reach the complete air-dry stage. The samples were scanned with a snapscan hyperspectral SWIR camera (manufactured by Imec, and slightly different from the one used on the heritage sample). The camera has a spectral range spanning from 1100 to 1670 nm, a spectral resolution of approximately 5 nm, and a total of 113 spectral bands. All six sides were scanned, the time interval between two consecutive measurements on the same side was approximately 16 mins. Due to variations in pore size distribution, the drying process varies from side to side. In Figure 5, the mean spectral reflectances of all measured samples obtained from one side of the cube are plotted, along with their corresponding WC.

3. Methodology

3.1. Spectral mixture analysis

In this work, we propose a methodology to accurately estimate the WC of wet samples from hyperspectral reflectance, making use of the fact that the optical properties of water-bearing materials are dominated by water in the SWIR wavelength region (1000 nm to 2500 nm). As indicated in Section 1, the spectral reflectance of a wet sample is significantly influenced by the distribution of water within the sample. This effect is observable, for instance, by absorption bands of molecular water around 1400 nm and 1900 nm (see Figures 2, 3 (b) and 5). In general, an increase in WC results in a deeper manifestation of the water absorption bands. The most pronounced valleys are observed when the sample is water saturated.

The main idea of the proposed methodology is to treat the problem as a binary mixture problem. The data manifold sampled by a number of wet samples with varying WC is a curve between the air-dry and saturated samples. The relative position of the reflectance spectrum of a test sample on this curve is a measure for its WC. To relate this relative position to its actual WC, it should be calibrated with respect to 2 samples on the curve (endmembers) with known reflectance spectra and WC (obtained from gravimetry). These endmembers correspond to a maximally wet sample ($\mathbf{e}_{\max}$) and a minimally wet sample ($\mathbf{e}_{\min}$). The choice of these endmembers depends on the application at hand. The widest range is obtained by choosing an air-dry

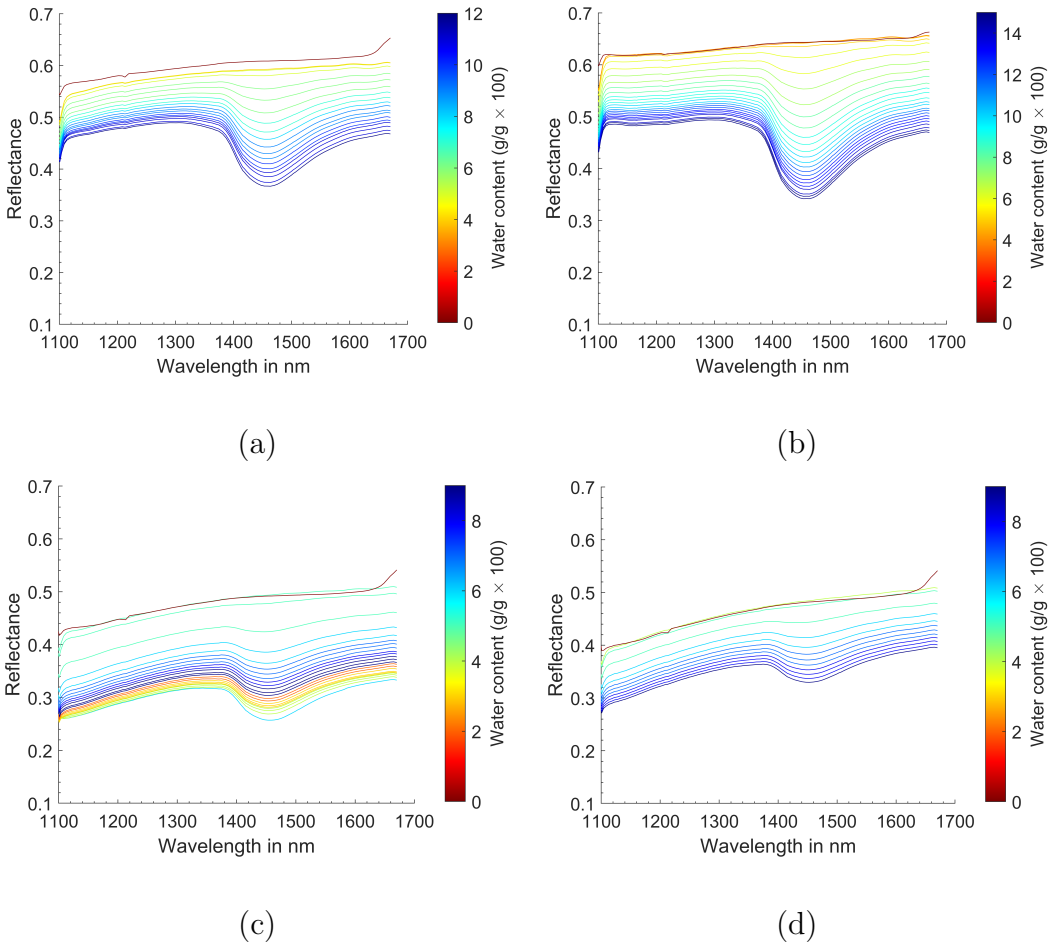

Figure 5: Measured reflectance spectra (SWIR camera) and corresponding WCs (see colorbar): (a) Red brick, (b) Yellow brick, (c) Grey brick 1, and (d) Grey brick 2.

and a saturated sample as endmembers. However, a more accurate WC estimation can be obtained when choosing a narrower range of interest between the endmembers.

3.2. Geodesic distance estimation

The relative position of a sample can be estimated by calculating the geodesic distance between the sample and the endmembers. In [19], the same principle was applied to the problem of binary intimate mixtures, where the curve was sampled with a large number of mixtures to approximate the geodesic distances. However, in practical scenarios, usually only one test sample and the two endmembers are available. Another challenge is that the acquired reflectance spectra in real-life scenarios are impaired by changes in acquisition conditions, such as illumination conditions and distance and orientation from the sensor. These effects mostly cause a random scaling of the measured reflectance spectra.

Both challenges can be solved by projecting all reflectance spectra onto the unit hypersphere, ensuring they are normalized to unit length. This removes all scaling effects. Moreover, on the unit hypersphere, the arc length (geodesic distance) between any two spectra can simply be computed by the arc cosine of their dot product. It is however not guaranteed that the spectrum $\mathbf{y}$ of a wet sample lies on the arc connecting the endmembers (as illustrated in Figure 6). In that case, $\mathbf{y}$ has to be projected on the arc connecting the endmembers (as indicated by the red curve) to determine its relative position. By using the law of cosines:

$$\begin{aligned} \cos\,(c_1) &= \cos\,(d)\,\cos\,(b_1) \\ \cos\,(c_2) &= \cos\,(d)\,\cos\,(b_2) \end{aligned} \tag{2}$$

the true arc lengths can be obtained without the need to explicitly project the data points onto the red curve:

$$b_1 = \arccos\left(\frac{\sin(T)}{\sqrt{\left[\left[\frac{\cos\,(c_2)}{\cos\,(c_1)} - \cos\,(T)\right]^2 + \sin^2(T)\right]}}\right) \tag{3}$$

where $T = b_1 + b_2 = \arccos(\mathbf{e}_{\max}^T \mathbf{e}_{\min})$. The relative arc lengths are then

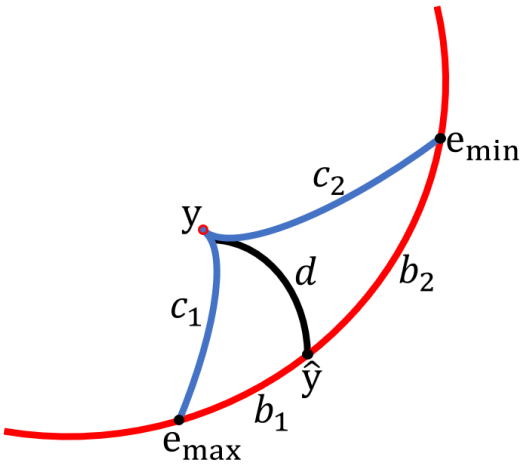

Figure 6: Red curve: arc connecting the two endmembers; Blue curves: the arcs connecting the wet sample ($\mathbf{y}$) with the endmembers. c_1 and c_2 denote the arc lengths between $\mathbf{y}$ and the endmembers $\mathbf{e}_{\text{max}}$ and $\mathbf{e}_{\text{min}}$, respectively. $\hat{\mathbf{y}}$ denotes the projection of $\mathbf{y}$ on the arc, and b_1 and b_2 denote the true arc lengths between $\hat{\mathbf{y}}$ and the endmembers.

determined as:

$$\hat{\mathbf{a}} = \begin{bmatrix} \frac{b_2}{b_1+b_2} \\ \\ \frac{b_1}{b_1+b_2} \end{bmatrix} \tag{4}$$

where $\hat{\mathbf{a}}$ is the vector containing the relative arc lengths of the sample between the maximally and the minimally wet endmember respectively.

3.3. Estimating water content

In the next step, the WC of the test sample (WC_y) is obtained as:

$$\text{WC}_\text{y} = \hat{a}_1 \times \text{WC}_\text{max} + \hat{a}_2 \times \text{WC}_\text{min} \tag{5}$$

where WC_max and WC_min denote the WC of the maximally and minimally wet endmembers, respectively.

3.4. Extrapolating water content

While we may have prior knowledge of the WC range of interest for a particular application, it cannot be ensured that all test samples will fall within the specified WC range [WC_min, WC_max]. When the WC of a test

sample is outside of this range, the proposed procedure will project the test sample on either one of the endmembers, leading to a large error in the estimated WC.

To find out whether the wet sample is inside or outside the range, we will make use of the high correlation between the thickness of the water layer within the sample and the WC, and we will employ a simple physical model to determine the thickness of the water layer. The primary assumption underlying this model is that a wet sample can be treated as a two-layer mixture containing water and a dry sample. This model relates the spectral reflectance of the wet sample ($\mathbf{y}$) to the spectral reflectance of the dry sample ($\mathbf{e}_{\text{dry}}$) using the following equation (refer to [20] for a detailed derivation):

$$\mathbf{y} = \mathbf{e}_{\text{dry}} \odot \exp(-\mathbf{a}L_{\mathbf{y}}) \tag{6}$$

where $\mathbf{a}$ is the absorption spectrum of water, $L_{\mathbf{y}}$ is the thickness of the layer of water, and $\odot$ is the elementwise multiplication of two vectors. While the absorption spectrum of water, as determined by a spectrophotometer, is publicly accessible, it cannot be directly employed for estimating $L_{\mathbf{y}}$ in datasets acquired by a spectroradiometer or hyperspectral camera with different spectral response. Moreover, as previously noted, the acquired spectra may be subject to random scaling effects arising from variations in acquisition conditions. To account for these 2 challenges, Eq. (6) is improved, leading to the following optimization problem:

$$\begin{aligned} \hat{L}_{\mathbf{y}} = \arg\min_{L_{\mathbf{y}}} & \left|\left| \frac{\mathbf{y}}{\|\mathbf{y}\|} - \frac{\mathbf{e}_{\text{dry}} \odot \text{SRF}(\exp(-\mathbf{a}L_{\mathbf{y}}))}{\|\mathbf{e}_{\text{dry}} \odot \text{SRF}(\exp(-\mathbf{a}L_{\mathbf{y}}))\|} \right|\right| \\ & \text{s.t.} : L_{\mathbf{y}} \geq 0 \end{aligned} \tag{7}$$

where SRF represents the spectral response function of the sensor utilized for obtaining the spectral reflectance of the wet sample and $\|\cdot\|$ computes the length of the vector.

With this procedure, the thickness of the layer of water in the test sample $\mathbf{y}$ ($L_{\mathbf{y}}$) and in both $\mathbf{e}_{\max}$ ($L_{\max}$) and $\mathbf{e}_{\min}$ ($L_{\min}$) are estimated. When $L_{\min} < L_{\mathbf{y}} < L_{\max}$, it can be anticipated that its WC falls within the predefined range, and the proposed procedure can be applied. In case $L_{\mathbf{y}}$ falls outside of the range $[L_{\min}, L_{\max}]$, an extrapolation procedure can be developed, as described in the next two sections.

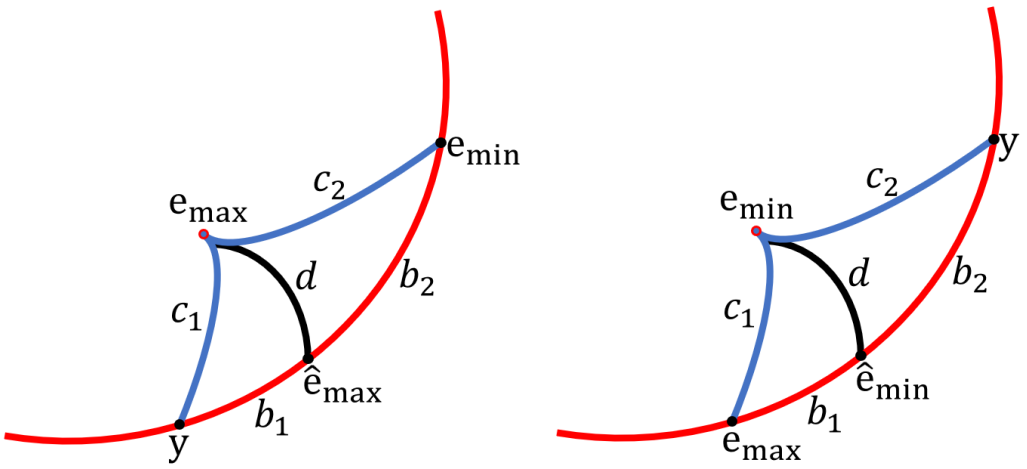

Figure 7: (a) Red curve: arc connecting $\mathbf{y}$ and $\mathbf{e}_{\text{min}}$; blue curves: the arcs connecting $\mathbf{e}_{\text{max}}$ with $\mathbf{e}_{\text{min}}$ and $\mathbf{y}$. $\hat{\mathbf{e}}_{\text{max}}$ denotes the projection of $\mathbf{e}_{\text{max}}$ on the arc; (b) Red curve: arc connecting $\mathbf{y}$ and $\mathbf{e}_{\text{max}}$; blue curves: the arcs connecting $\mathbf{e}_{\text{min}}$ with $\mathbf{e}_{\text{max}}$ and $\mathbf{y}$. $\hat{\mathbf{e}}_{\text{min}}$ denotes the projection of $\mathbf{e}_{\text{min}}$ on the arc.

3.4.1. $\text{L}_{\text{max}} < \text{L}_{\mathbf{y}}$

In this case, the WC of the test sample $\mathbf{y}$ is expected to exceed that of the maximally wet sample ($\mathbf{e}_{\text{max}}$) (see Figure 7 (a)). Now, $\mathbf{y}$ and $\mathbf{e}_{\text{min}}$ can be considered as the two extremes, and the WC of $\mathbf{e}_{\text{max}}$ can be determined from:

$$\text{WC}_{\text{max}} = \hat{a}_1 \times \text{WC}_{\text{y}} + \hat{a}_2 \times \text{WC}_{\text{min}} \tag{8}$$

where $\hat{a}_1$ and $\hat{a}_2$ are obtained from Eq. (4). From this, the WC of the test sample is then derived as:

$$\text{WC}_{\text{y}} = \frac{\text{WC}_{\text{max}} - \hat{a}_2 \times \text{WC}_{\text{min}}}{\hat{a}_1} \tag{9}$$

3.4.2. $\text{L}_{\mathbf{y}} < \text{L}_{\text{min}}$

In this case, the WC of the test sample $\mathbf{y}$ is expected to be lower than that of the minimally wet sample ($\mathbf{e}_{\text{min}}$) (see Figure 7 (b)). Now, $\mathbf{e}_{\text{max}}$ and $\mathbf{y}$ can be considered as the two extremes, and the WC of $\mathbf{e}_{\text{min}}$ can be determined

from:

$$\mathrm{WC}_{\mathrm{min}} = \hat{a}_1 \times \mathrm{WC}_{\mathrm{max}} + \hat{a}_2 \times \mathrm{WC}_{\mathrm{y}} \tag{10}$$

From this, the WC of the test sample is then derived as:

$$\mathrm{WC}_{\mathrm{y}} = \frac{\mathrm{WC}_{\mathrm{min}} - \hat{a}_1 \times \mathrm{WC}_{\mathrm{max}}}{\hat{a}_2} \tag{11}$$

4. Experiments and Results

The proposed approach will be referred to as EWCE (efficient water content estimator). The proposed method EWCE is validated on the datasets, described in section 2. The performance of EWCE will be compared to the same estimation procedure using the full range of WC, i.e., where the end-members correspond to the saturated sample and the dry sample. This approach will be referred to as NRAL (this method was applied to the problem of soil moisture content in our earlier work [21]):

$$\mathrm{WC}_{\mathrm{y}} = \hat{a}_1 \times \mathrm{WC}_{\mathrm{sat}} + \hat{a}_2 \times \mathrm{WC}_{\mathrm{dry}} = \hat{a}_1 \times \mathrm{WC}_{\mathrm{sat}} \tag{12}$$

where $\mathrm{WC}_{\mathrm{sat}}$ and $\mathrm{WC}_{\mathrm{dry}}$ denote the WC of the saturated and dry samples, respectively.

Quantitative comparisons are presented using the root mean squared error (RMSE), which represents the error between the estimated WC ($\hat{\mathrm{WC}}$) and the actual WC (WC):

$$\mathrm{RMSE} = \sqrt{\frac{1}{N}\sum_{i=1}^{N}\left(\hat{\mathrm{WC}}_i - \mathrm{WC}_i\right)^2} \times 100 \tag{13}$$

where N is the number of test spectra.

For an accurate estimation of the WC from spectral reflectance, an additional problem arises, as the bulk ground truth WC may not be adequately represented in the acquired datasets, especially for samples with low WC. As water evaporates at the surface, the WC of a sample is not homogeneously distributed. Considering the low information depth of the spectral reflectance within the optical wavelengths (400 nm to 2500 nm) [12], which varies between a few micrometers and a few hundred micrometers, depending on the chemical composition and porosity of the samples, the estimated WC

may deviate from the bulk WC. We observed that the spectra of air-dried samples and samples with approximately 5 (g/g ×100) WC are very similar (see Figure 8). To limit discrepancies between the ground-measured WC and estimated WC from spectral reflectance, all analyzes will be limited to WC values higher than 5 (g/g ×100).

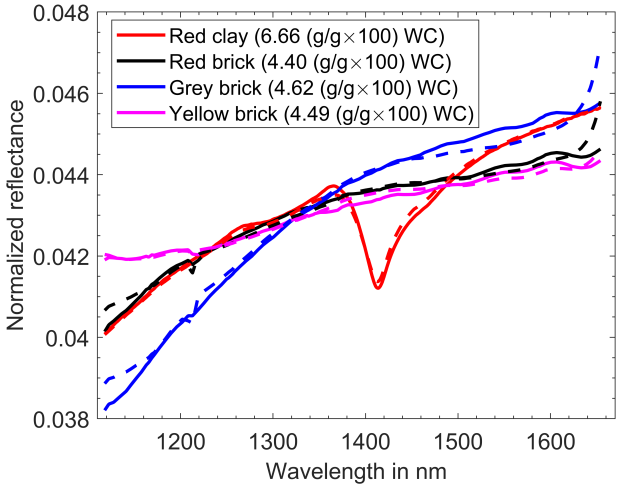

Figure 8: Spectra of air-dry samples (dashed lines) and samples with approximately 5 (g/g ×100) WC (full line).

Two groups of experiments were performed to validate the proposed approach in different conditions. In the first group of experiments, the accuracy of the proposed approach within a narrow WC range was explored. Endmembers in this study were selected with the minimum and maximum WC levels within a specified narrow range. In the second experiment, we validated the proposed method on samples falling outside of the specified WC range [WC_{min}, WC_{max}].

4.1. Interpolating water content experiments

In the first group of experiments, the methods are applied to estimate the WC of test samples within a specified WC range. Using the proposed approach, endmembers with the minimum and maximum WC of the range were chosen, while NRAL used the endmembers of an air-dry and saturated sample.

4.1.1. Wet clay samples experiment

For this dataset, all WC ranges that are multiples of 10 (g/g ×100) between a WC of 10 (g/g ×100) and a WC around saturation (i.e., 70 (g/g ×100) for Roof and Mixed clays and 50 (g/g ×100) for Red clay) were evaluated. The results are shown in Figure 9.

The outcome of the experiments can be summarized as follows:

- EWCE outperformed NRAL in estimating WC for all three clays, with the exception of a few specific WC ranges for Roof clay (i.e, 30-60 (g/g ×100), 30-70 (g/g ×100), 40-60 (g/g ×100), 40-70 (g/g ×100), and 50-70 (g/g ×100)).
- The RMSE of EWCE is 2-5 times lower than that of NRAL for all three clays.
- In general, EWCE produced the lowest errors on the narrow ranges (10-20 (g/g ×100), 20-30 (g/g ×100), 30-40 (g/g ×100), 40-50 (g/g ×100), 50-60 (g/g ×100), and 60-70 (g/g ×100)). Within these specified ranges, the RMSE varied between 0.40-2.66% for Roof clay, 0.52-2.54% for Red clay, and 0.21-2.48% for Mixed clay.

4.1.2. Wet built heritage sample experiment

For this dataset, all ranges that are multiples of 2 (g/g ×100) between a WC of 5 (g/g ×100) and a WC around saturation (i.e., 17 (g/g ×100)) were evaluated. From each hyperspectral image corresponding to a specific WC, all brick pixels were averaged for further processing. The results are shown in Figure 10. The RMSE of EWCE generally remained well below 0.5% across all WC ranges, while NRAL produced errors up to more than 4%.

4.1.3. Wet brick samples experiment

On this dataset, all WC ranges that are multiples of 1 (g/g ×100) for Grey bricks, 1.5 (g/g ×100) for Red brick, and 2 (g/g ×100) for Yellow brick were evaluated. The lowest WC that was considered was 5 (g/g ×100) and the highest was a WC around saturation (i.e., 9 (g/g ×100) for Grey bricks, 11 (g/g ×100) for Red brick, and 15 (g/g ×100) for Yellow brick). From each hyperspectral image corresponding to a specific WC, all pixels were averaged to estimate the WC. As these brick samples were scanned from all six sides, the obtained RMSE's for each side were averaged over all 6 sides.

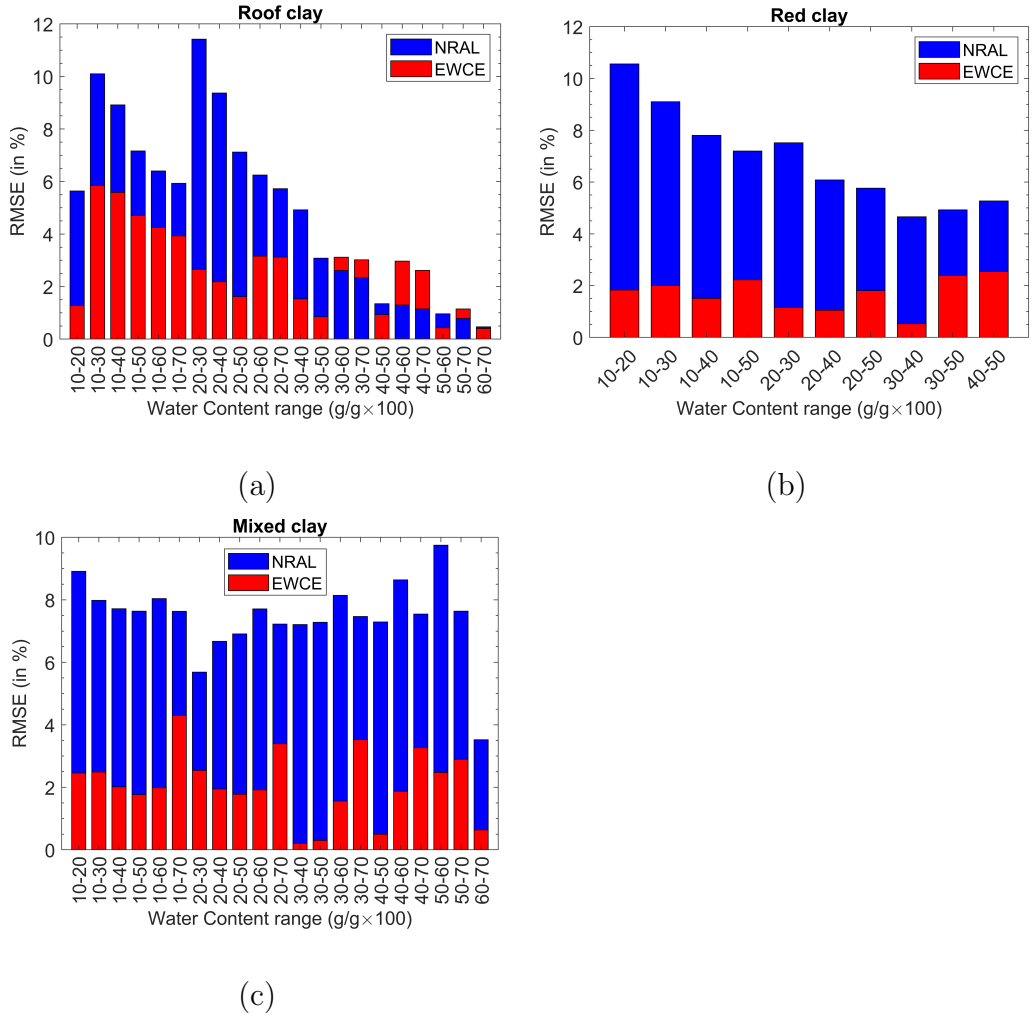

Figure 9: Results of NRAL and the proposed approach in terms of RMSE (%) for different WC ranges: (a) Roof clay, (b) Red clay, and (c) Mixed clay.

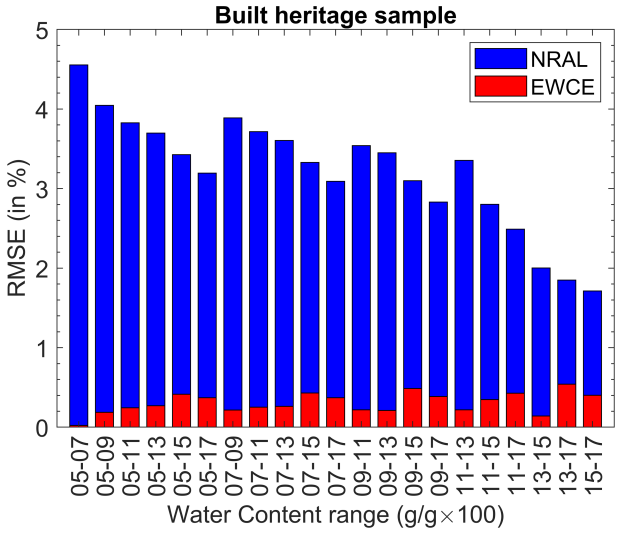

Figure 10: Results of NRAL and the proposed approach in terms of RMSE (%) for different WC ranges on the built heritage sample.

The results are shown in Figure 11. EWCE outperforms NRAL for all four brick samples.

4.2. Extrapolating water content experiments

In the second group of experiments, the proposed method is applied to estimate the WC of test samples that fall outside of the WC range of the endmembers. Unlike the previous experiments, in this particular experiment, the proposed method requires next to the two endmember spectra, the spectrum of an air-dried sample, the absorption spectrum of pure water, and the SRF of the applied sensor, in order to estimate the water layer thickness. On the other hand, NRAL requires the spectral reflectances of air-dried and saturated samples as endmembers.

4.2.1. Wet clay samples

For the Roof and Mixed clays, the WC range for the endmembers was chosen to be 30-50 (g/g $\times$100), while for Red clay, it was chosen to be 20-40 (g/g $\times$100). The results are shown as a scatterplot in Figure 12. In general, the results obtained by extrapolating the WC outside of the considered WC range (red stars) are slightly inferior to those within the WC range (red

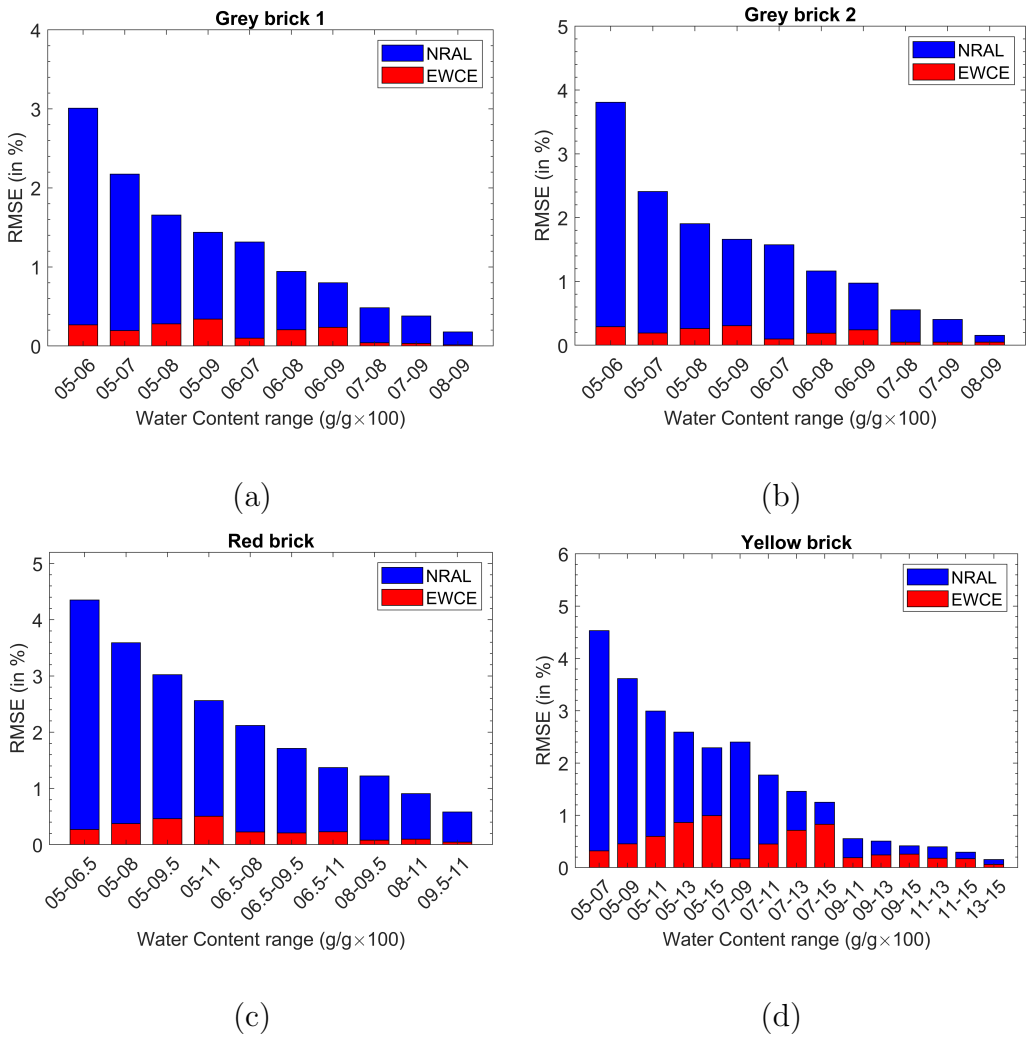

Figure 11: Results of NRAL and the proposed approach in terms of RMSE (%) for different WC ranges: (a) Grey brick 1, (b) Grey brick 2, (c) Red brick, and (d) Yellow brick.

hollow circles). With the exception of a few test samples from the Roof clay, the proposed method outperformed NRAL.

4.2.2. Built heritage sample

In the final experiment, we applied our extrapolation method to accurately estimate the WC of the wet built heritage sample. The WC range for the endmembers was chosen to be 10-13 (g/g $\times$100). The results are shown as a scatterplot in Figure 13. It can be observed that the performance of EWCW is high, whether outside or inside the considered WC. The result obtained by NRAL deviates considerably from the 1:1 line.

5. Discussion

From the experimental results, the following observations can be made:

- The proposed approach EWCE is a robust algorithms for accurately estimating the WC of wet samples from their spectral reflectance. The algorithm has been designed to be invariant to variations in acquisition conditions. Even when the considered WC range is the entire range from dry to saturated WC values (NRAL), the method is efficient.

- To estimate the WC of a sample, NRAL requires the spectral reflectance of both an air-dried and a saturated sample along with their corresponding WCs. On the other hand, EWCE requires the spectral reflectance of a minimally wet and a maximally wet sample along with their WCs, the spectrum of an air-dried sample, the absorption spectrum of pure water, and the SRF of the sensor.

- In general, EWCE outperformed NRAL across all datasets. NRAL obtained an average error of 1.6% on the brick samples, 3.2% on the built heritage sample, and 6.3% on the clay samples. EWCE obtained an average error of 0.28% on the brick samples, 0.31% on the built heritage sample, and 2.2% on the clay samples.

- The relatively large error of NRAL arises from a systematic bias of approximately 5 (g/g $\times$100) WC that occurs in most of the datasets. This is due to the lack of water content information in the spectral reflectance of samples with low WC (see Figure 8). The performance of NRAL can thus be improved by replacing the air-dry endmember by

an endmember with 5 (g/g $\times$100) WC. This can be observed from the results on the brick dataset in Figure 11 (see results for the 5-9 (g/g $\times$100) WC range for the Grey bricks, the 5-11 (g/g $\times$100) WC range for the Red brick, and the 5-15 (g/g $\times$100) WC range for the Yellow brick). To further illustrate this, Figure 14 compares the obtained scatterplots with WC range 5-17 (g/g $\times$100) and with WC range 0-17 (g/g $\times$100) on the built heritage sample.

- The major advantage of using a hyperspectral camera over a spectroradiometer is the availability of an entire image of reflectance spectra. This allows to generate spatially resolved WC maps, visualizing spatial variations of WC due to heterogeneities in e.g., pore size distribution of brick samples. As an illustration, Figure 15 displays a WC map obtained by EWCE of the built heritage sample with a measured ground truth bulk WC of approximately 11 (g/g $\times$100). As can be observed, the estimated WC spatially varies between 8-15 (g/g $\times$100).

- A disadvantage of the proposed approach is that the method can not be applied to materials that chemically react with water. In that sense, it will not work for concrete, as part of the water will chemically react, while the proposed method only allows the estimation of the free water. Although not strictly limited to inorganic materials, we are reluctant to apply the approach to wood, where the water distribution is expected to be highly inhomogeneous. In future work, we will investigate the extension of the proposed work to estimate WC of a wider range of building materials (e.g., concrete and wood).

- The major limitation of the proposed method is the requirement of a dry and a wet endmember for each material type. To alleviate this requirement, it is crucial to obtain information about the porosity of the sample, pore sizes, and their distributions. Currently, we are exploring effective non-destructive methods to acquire this information.

6. Conclusion

In this work, a nondestructive methodology was developed to accurately estimate the water content of building materials from shortwave infrared spectral reflectance. The method allows a continuous, spatially resolved

monitoring of water content, and is by design invariant to variations in acquisition conditions. Validation on different datasets of clay powders and bricks provided confirmation of the effectiveness of the proposed method.

Acknowledgement

The research presented in this paper is funded by the Research Foundation-Flanders - project G031921N. Bikram Koirala is a postdoctoral fellow of the Research Foundation Flanders, Belgium (FWO: 1250824N-7028). We would like to clarify that this paper is based on the methodology outlined in the patent application that we filed recently.

References

[1] L.-O. Nilsson, *Methods of Measuring Moisture in Building Materials and Structures*. Springer International Publishing, 2018.

[2] E. Piuzzi, E. Pittella, S. Pisa, A. Cataldo, E. De Benedetto, and G. Cannazza, "Microwave reflectometric methodologies for water content estimation in stone-made cultural heritage materials," *Measurement*, vol. 118, pp. 275–281, 2018.

[3] M. Bensalem, A. Sommier, J. C. Mindeguia, J. C. Batsale, and C. Pradere, "Estimation of the diffusion coefficient of hygroscopic materials using a contactless transient thz water vapour content imaging and excitation device," *International Journal of Heat and Mass Transfer*, vol. 208, 2023.

[4] E. Nazemi, M. Dinca, A. Movafeghi, B. Rokrok, and M. H. C. Dastjerdi, "Estimation of volumetric water content during imbibition in porous building material using real time neutron radiography and artificial neural network," *Nuclear Instruments & Methods in Physics Research Section A-Accelerators Spectrometers Detectors and Associated Equipment*, vol. 940, pp. 344–350, 2019.

[5] Q. Zhaxi, H. Zhou, Z. Long, J. Guo, Y. Zhou, and Z. Zhang, "Non-destructive measurement of the water content in building materials by single-sided nmr-mouse," *Sustainability*, vol. 15, no. 14, 2023.

[6] D. Lobell and G. Asner, "Moisture effects on soil reflectance," *Soil Science Society of America Journal*, vol. 66, no. 3, pp. 722–727, 2002.

[7] R. M. Hoffer and C. J. Johannsen, "Ecological potential in spectral signatures analysis," *Remote Sensing in Ecology*, pp. 1–16, 1969.

[8] R. Colombo, M. Merom, A. Marchesi, L. Busetto, M. Rossini, C. Giardino, and C. Panigada, "Estimation of leaf and canopy water content in poplar plantations by means of hyperspectral indices and inverse modeling," *Remote Sensing of Environment*, vol. 112, no. 4, pp. 1820–1834, 2008.

[9] D. Li, W. Yu, H. Zheng, C. Guo, X. Yao, Y. Zhu, W. Cao, and T. Cheng, "Towards practical semi-empirical models for the estimation of leaf and canopy water contents from hyperspectral reflectance," *Computers and Electronics in Agriculture*, vol. 214, 2023.

[10] X. Ge, J. Wang, J. Ding, X. Cao, Z. Zhang, J. Liu, and X. Li, "Combining uav-based hyperspectral imagery and machine learning algorithms for soil moisture content monitoring," *Peerj*, vol. 7, 2019.

[11] A. Dupiau, S. Jacquemoud, X. Briottet, S. Fabre, F. Viallefont-Robinet, W. Philpot, C. Di Biagio, M. Hebert, and P. Formenti, "Marmit-2: An improved version of the marmit model to predict soil reflectance as a function of surface water content in the solar domain," *Remote Sensing of Environment*, vol. 272, 2022.

[12] M. Sadeghi, S. B. Jones, and W. D. Philpot, "A linear physically-based model for remote sensing of soil moisture using short wave infrared bands," *Remote Sensing of Environment*, vol. 164, pp. 66–76, 2015.

[13] S. Rath and Y. Sakai, "Evaluation of the water penetration depth in mortar using water indicator and hyperspectral imaging," *Construction and Building Materials*, vol. 380, 2023.

[14] M. Ghandehari, C. S. Vimer, I. Ioannou, A. Sidelev, W. Jin, and P. Spellane, "In-situ measurement of liquid phase moisture in cement mortar," *NDT & E International*, vol. 45, no. 1, pp. 162–168, 2012.

[15] Z. Zahiri, D. F. Laefer, and A. Gowen, "The feasibility of short-wave infrared spectrometry in assessing water-to-cement ratio and density of

hardened concrete," *Construction and Building Materials*, vol. 185, pp. 661–669, 2018.

[16] K. Lee, J. J. Park, and G. Hong, "Prediction of ground water content using hyperspectral information through laboratory test," *Sustainability*, vol. 14, no. 17, 2022.

[17] J. Melada, P. Arosio, M. Gargano, I. Veronese, S. Gallo, and N. Ludwig, "Optical reflectance apparatus for moisture content determination in porous media," *Microchemical Journal*, vol. 154, 2020.

[18] E. Rosina, "When and how reducing moisture content for the conservation of historic building. a problem solving view or monitoring approach?" *Journal of Cultural Heritage*, vol. 31, pp. S82–S88, 2018.

[19] B. Koirala, Z. Zahiri, A. Lamberti, and P. Scheunders, "Robust supervised method for nonlinear spectral unmixing accounting for endmember variability," *IEEE Transactions on Geoscience and Remote Sensing*, vol. 59, no. 9, pp. 7434–7448, 2021.

[20] B. Koirala, N. Mboga, R. Moelans, E. Knaeps, S. Sels, F. Winters, S. Samsonova, S. Vanlanduit, and P. Scheunders, "Study on the potential of oil spill monitoring in a port environment using optical reflectance," *Remote Sensing*, vol. 15, no. 20, 2023.

[21] B. Koirala, Z. Zahiri, and P. Scheunders, "A robust supervised method for estimating soil moisture content from spectral reflectance," *IEEE Transactions on Geoscience and Remote Sensing*, vol. 60, pp. 1–13, 2022.

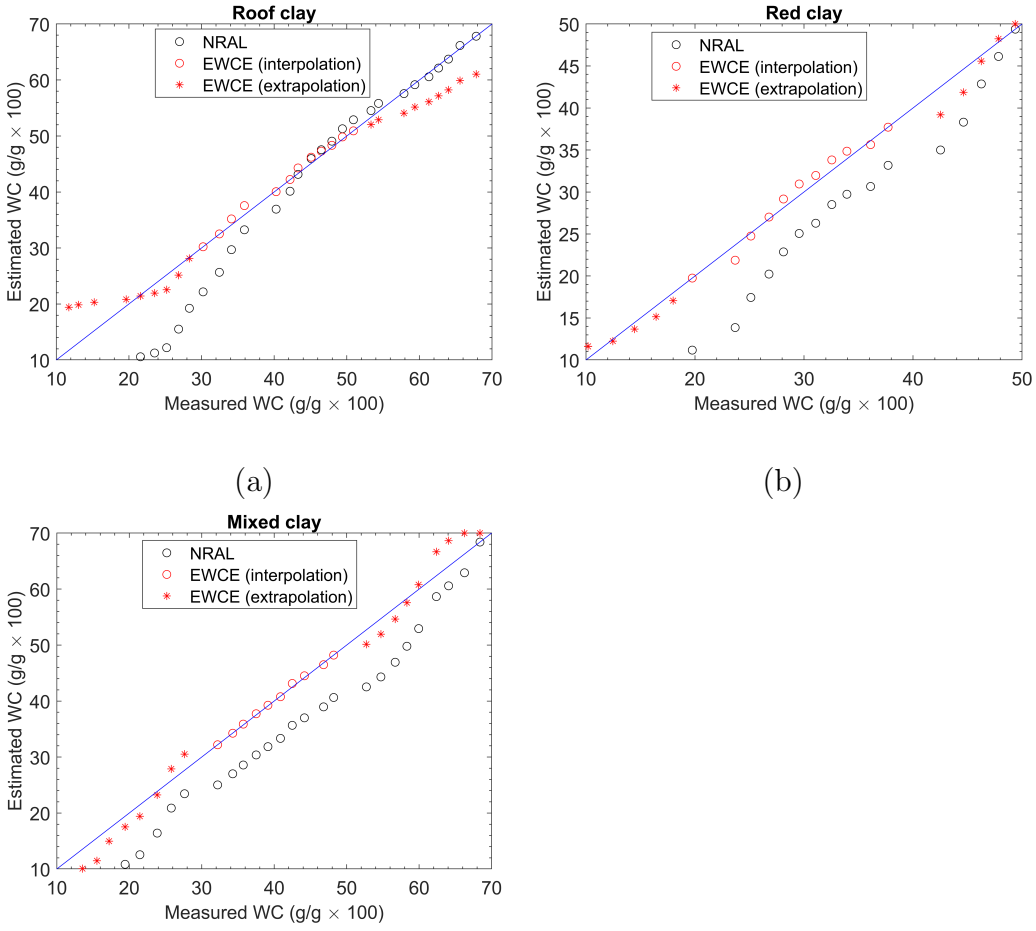

Figure 12: Estimated WC versus measured ground truth WC of the clay samples: (a) Roof clay ($\mathbf{e}_{\min}$: 30 (g/g ×100) WC and $\mathbf{e}_{\max}$: 50 (g/g ×100) WC), (b) Red clay ($\mathbf{e}_{\min}$: 20 (g/g ×100) WC and $\mathbf{e}_{\max}$: 40 (g/g ×100) WC), and (c) Mixed clay ($\mathbf{e}_{\min}$: 30 (g/g ×100) WC and $\mathbf{e}_{\max}$: 50 (g/g ×100) WC).

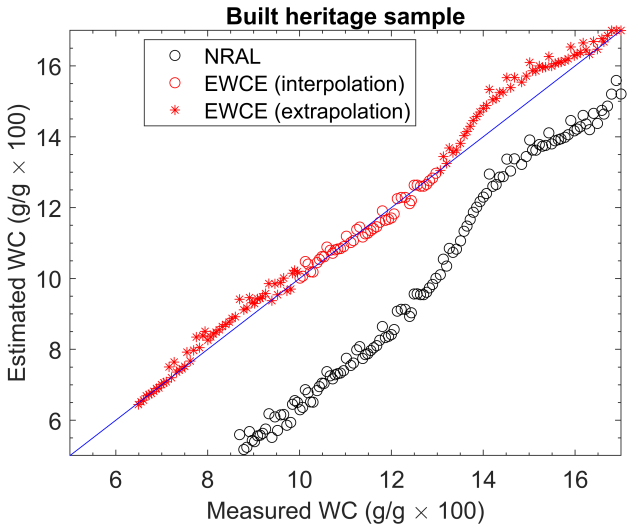

Figure 13: Estimated WC versus measured ground truth WC of the built heritage sample ($\mathbf{e}_{\min}$: 10 (g/g ×100) WC and $\mathbf{e}_{\max}$: 13 (g/g ×100) WC).

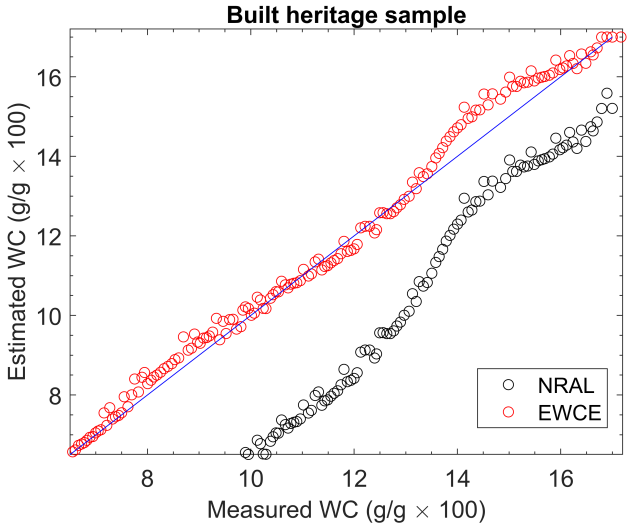

Figure 14: Estimated WC versus measured ground truth WC of the built heritage sample. EWCE ($\mathbf{e}_{\min}$: 5 (g/g ×100) WC and $\mathbf{e}_{\max}$: 17 (g/g ×100) WC); NRAL ($\mathbf{e}_{\min}$: 0 (g/g ×100) WC and $\mathbf{e}_{\max}$: 17 (g/g ×100) WC)

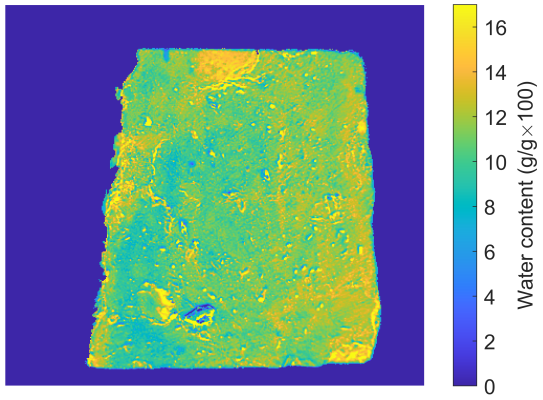

Figure 15: WC map of the built heritage sample with an approximate measured WC of 11% ($\mathbf{e}_{\min}$: 10 (g/g ×100) WC and $\mathbf{e}_{\max}$: 13 (g/g ×100) WC).